Neutron-scattering studies of the geometrically frustrated spinel $LiMn_2O_4$

J. E. Greedan,[1] C. R. Wiebe,[2] A. S. Wills,[3] and J. R. Stewart[3]
[1]*Brockhouse Institute for Materials Research, Department of Chemistry, McMaster University, Hamilton, Canada*
[2]*Brockhouse Institute of Materials Research, Department of Physics, McMaster University, Hamilton, Canada*
[3]*Institut Laue-Langevin, Grenoble, France*
(Received 17 September 2001; published 2 May 2002)

The spinel structure oxide $LiMn_2O_4$, a geometrically frustrated antiferromagnet, was studied by neutron-scattering methods. Diffraction studies with unpolarized neutrons, $\lambda = 2.52$ Å and $E = 12.9$ meV, are consistent with $T_c = 65.5(5)$ K. In agreement with previous results both Bragg peaks, indicative of long-range order, and a broad Lorentzian feature, centered at $Q = 1.36$ Å^{-1}, indicative of short range order, coexist down to 2 K. The correlation length ξ associated with the short-range order is 3(1) Å, the order of the nearest-neighbor (nn) Mn-Mn distances. Quantitative estimates of the Bragg and Lorentzian contributions from 80 to 2 K indicate the growth of the Bragg at the expense of the Lorentzian component, that their integrated intensities become essentially equal below 20 K and that the total magnetic scattering is conserved within the *E*-transfer *Q* range studied. Further studies with neutron polarization analysis, using neutrons with $\lambda = 4.8$ Å and 3.55 meV, quantitatively measure the total differential magnetic cross section, $d\sigma_{mag}/d\Omega$ to be 1.05 b sr^{-1} f.u.$^{-1}$ at 1.5 K, which is close to the value expected for a static spin model. $d\sigma_{mag}/d\Omega$ increases by about 20% between 120 and 1.5 K below T_c, suggesting significant spin dynamics for $T > T_c$, which lie outside of the energy window of the neutron polarization analysis experiment. In addition, above T_c the Lorentzian peak broadens slightly and the center shifts from 1.36 Å^{-1} at 80 K to 1.29 Å^{-1} at 120 K. Inelastic magnetic scattering was measured using neutron polarization analysis over the energy range +2.0 to −4.9 meV at 1.5 and 80 K. At 1.5 K the scattering is essentially elastic with at most ~23% of the spins fluctuating while at 80 K it is largely inelastic with at least 75% of the spins fluctuating. These results are consistent with the existence of a correlated paramagnetic state above T_c, which evolves with decreasing temperature into a ground state below 20 K in which about half the spins are long-range ordered and the other half are in a spin-glass-like configuration. This is in turn consistent with the presence of partial charge ordering between Mn^{3+} and Mn^{4+} in the low-temperature structure of $LiMn_2O_4$ and the inherent geometrical frustration of the Mn sublattice.

DOI: 10.1103/PhysRevB.65.184424 PACS number(s): 75.25.+z, 61.12.−q, 75.50.Lk, 75.40.Gb

I. INTRODUCTION

While the cubic spinel $LiMn_2O_4$ has been studied intensively as a candidate cathode material in lithium solid-state batteries,[1–5] attention has recently turned to the fundamental electronic and magnetic properties of it and the closely related series $Li_xMn_2O_4$ (where $0 \leqslant x \leqslant 2$).[8–17] Materials with these compositions can be formed by the removal or insertion of Li by the use of either electrochemical or so-called ''soft chemical'' techniques. By use of these techniques all the compositions between the limiting members λ-MnO_2 and $Li_2Mn_2O_4$ can be synthesized. These all retain the Mn sublattice topology of the *B*-site spinel, a network of corner-sharing tetrahedra, often called the pyrochlore lattice, which in the presence of nearest-neighbor antiferromagnetic exchange interactions, leads to geometric frustration.[6,7] The importance of geometrical frustration is exemplified by the complex magnetic properties of λ-MnO_2, which orders with the propagation vector $\mathbf{k} = (\frac{1}{2}\,\frac{1}{2}\,\frac{1}{2})$ (256 spins per magnetic cell) observed below 32 K,[12] and by the absence of long-range magnetic order in $Li_2Mn_2O_4$. The latter is remarkable in that it has been found to possess only two-dimensional spin correlations down to 1.6 K in spite of the $3d$ Mn sublattice.[13]

$LiMn_2O_4$ exhibits even more complex behavior. Above 280 K stoichiometric $LiMn_2O_4$ crystallizes in the ideal cubic spinel structure with 50% Mn^{3+} and 50% Mn^{4+} distributed randomly over the octahedral ($16d$) sites of the $Fd3m$ space group and Li^+ in the tetrahedral ($8b$) sites. Below 280 K a first-order structural phase transition occurs that results in an orthorhombic structure, *Fddd*, with a large supercell, $a \approx b \approx 3a_{cub}$ and $c \approx c_{cub}$.[17,19,20] This transition appears to be driven by a partial charge ordering between Mn^{3+} and Mn^{4+} among the distinct Mn sites.[17,19] The resulting structure is stable down to at least 10 K. The bulk magnetic properties of $LiMn_2O_4$ are quite complex with field-cooled (FC), zero-field-cooled (ZFC) divergences, typical of a spin-glass-like magnetic ground state, being present below 65 K.[14–16] Previous neutron diffraction studies demonstrated not only the appearance of Bragg peaks that are indicative of the onset of long-range magnetic order below 65 K, but also a broad, diffuse feature at finite *Q* that is characteristic of short-range antiferromagnetic order and which persists above 70 K. These observations are corroborated by at least one other neutron diffraction study[17] but not by a second[18] where no Bragg peaks are seen down to 8 K. Remarkably, both the Bragg peaks and the diffuse background coexist down to 10 K.[14] Preliminary indexing of the magnetic Bragg peaks indicates that the magnetic unit cell is very large, it may contain 1152 spins, and the structure has not yet been solved.[14]

Other oxide spinels show similar behavior, such as $ZnFe_2O_4$ and $ZnCr_2O_4$ (Refs. 21–23). In this study a more

detailed examination of the complex magnetism in $LiMn_2O_4$ was made using both elastic and inelastic neutron scattering with polarized and unpolarized beams. In particular, the use of polarization analysis permitted a quantitative measure of the total magnetic cross section to be made for the first time. The inelastic neutron polarization analysis data address the issue of whether the diffuse feature is a static or dynamic phenomenon.

II. EXPERIMENT

A. Sample preparation

$LiMn_2O_4$ was prepared by reaction of Li_2CO_3 and Mn_2O_3 in air with the following heating schedule: room temperature to 650 °C over 3 h, hold at 650 °C for 12 h, heat to 800 °C over 3 h, hold at 800 °C for 12 h. The sample used in these experiments had a mass of 13.8 g.

The lattice constant of the room-temperature cubic phase was found to be $a=8.2444(5)$ Å from x-ray Guinier-Hågg camera data, in excellent agreement with literature values.[19]

B. Unpolarized neutron diffraction

Data were collected at the Institut Laue-Langevin (ILL) on the instrument D1B using neutrons with a wavelength of $\lambda=2.52$ Å over the temperature range 2–80 K. Data taken up to 70 K were taken at 2 K intervals. The sample was held in a vanadium can with He exchange gas and a standard ILL ''orange'' He cryostat.

C. Neutron polarization analysis

Measurements were carried out at the ILL using the instrument D7 with the *xyz* polarization analysis technique. D7 features a 32 element multidetector. An incident wavelength of 4.84 Å was used, giving access to a Q range of 0.15–2.5 $Å^{-1}$. This instrument is described in detail in Ref. 21. Polarization of the incident neutron beam and the subsequent polarization analysis were achieved by the use of supermirror benders. In *xyz* polarization analysis the multidetector is a one-dimensional planar device, which defines the *x*-*y* plane. This geometry ensures that the scattering vector **Q** is always perpendicular to the *z* direction as required by the technique. Spin flip (SF) and non-spin flip (NSF) differential cross sections are then measured for the polarization of the incident beam in each of the *x*, *y*, and *z* directions, making a total of six measurements in all, labeled $d\sigma_{\mathrm{SF}}^{(x,y,z)}/d\Omega$ and $d\sigma_{\mathrm{NSF}}^{(x,y,z)}/d\Omega$. As no energy analysis was performed, these data are integrated over the energy-transfer window of the instrument, which is limited by the incident neutron energy (3.49 meV) on the energy loss side (downscattering) and by the vanishing transmission of the supermirror benders at around −10 meV on the energy gain side (upscattering). An absolute normalization of the data was achieved using a vanadium standard, so that the quantitative value of the differential magnetic cross section within the energy window of the experiment, $d\sigma_{\mathrm{magn}}/d\Omega$, in units of b sr^{-1} f.u.$^{-1}$ could be obtained from either

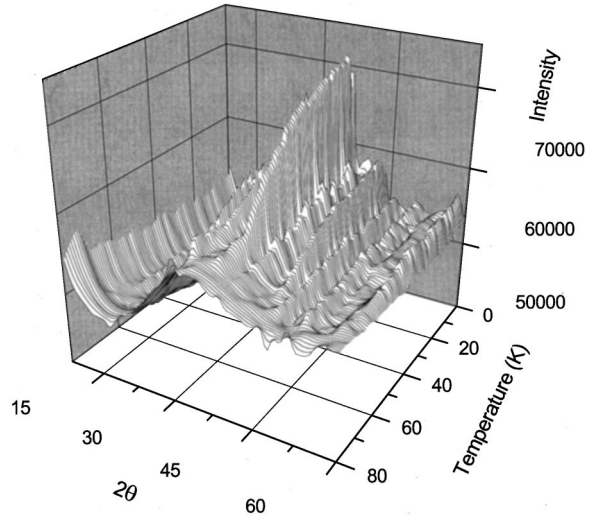

FIG. 1. Temperature evolution of magnetic scattering in $LiMn_2O_4$, D1B data with unpolarized neutrons, $\lambda=2.52$ Å.

$$\frac{d\sigma_{\mathrm{magn}}}{d\Omega}=\frac{d\sigma_{\mathrm{SF}}^{X}}{d\Omega}+\frac{d\sigma_{\mathrm{SF}}^{Y}}{d\Omega}-2\frac{d\sigma_{\mathrm{SF}}^{Z}}{d\Omega}$$

or

$$\frac{d\sigma_{\mathrm{magn}}}{d\Omega}=2\frac{d\sigma_{\mathrm{SF}}^{Z}}{d\Omega}-\frac{d\sigma_{\mathrm{SF}}^{X}}{d\Omega}-\frac{d\sigma_{\mathrm{SF}}^{Y}}{d\Omega}.$$

As the two combinations correspond to independent measurements, the magnetic differential cross section is taken as their average. More details on *xyz* polarization analysis are available in Refs. 22, 23. In this experiment 13.8 g. of $LiMn_2O_4$ were contained in an annular aluminum sample can. This configuration was chosen in order to minimize the total sample thickness to the beam, and thus problems due to the very large absorption of naturally present ^{6}Li. The transmission coefficient was 53%. Data were taken at 1.5, 30, 40, 50, 60, 70, 80, 90, and 120 K.

D. Neutron inelastic scattering with neutron polarization analysis

These measurements were also taken using the D7 instrument in the chopper-based time-of-flight (TOF) mode with incident neutron energy of 3.49 meV. The energy-transfer range covered in this configuration was from ~2 to ~−5 meV and data were taken at 1.5 and 80 K.

III. RESULTS AND DISCUSSION

A. Unpolarized neutron diffraction

Figure 1 shows the data in a three-dimensional plot for the investigated temperature (2–70 K) and 2θ ranges. The data are consistent with two previous reports that showed the development of sharp Bragg peaks below ~65 K superimposed on a very broad, diffuse background.[14,17] Figure 2 gives a more detailed view of the data at 70 and 2 K. There are only a few weak nuclear reflections within this range as seen in the 70 K data. The temperature dependence of the intensity

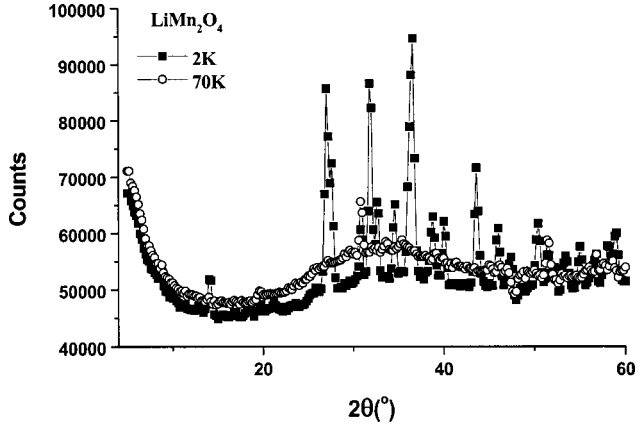

FIG. 2. Comparison of the 2 and 70 K D1B data for $LiMn_2O_4$, unpolarized neutrons, $\lambda = 2.52$ Å.

of the strong magnetic peak which is comprised of two or more Bragg reflections, near 27° in 2θ is shown in Fig. 3. These data are consistent with $T_c \approx 65$ K, as indicated by previously reported bulk susceptibility measurements.[14,15] Attempts were made to locate T_c more precisely by fitting the data near the apparent T_c assuming a critical phase transition, i.e., by fitting to the expression $I^{1/2} = At^{\beta}$, where $t = (T_c - T)/T_c$. Fits were carried out assuming a range of T_c's from 64.5 to 66.0 K in increments of 0.5 K over the temperature range 54–64 K. The quality of the fits as measured by the least squares residual was nearly indistinguishable for the choices 65.0 to 66.0. In all these cases the derived critical exponents were unusual and probably unphysical as their mean value, $\beta = 0.57(6)$, exceeds even the mean-field value of 0.50. Given the limited range of reduced temperature involved, the significance of this result is dubious and more detailed studies are warranted.

As already noted, the Bragg peaks are superimposed on a broad, diffuse background, which implies that a significant fraction of the spins are involved in short-range magnetic order even at the lowest temperatures studied, 2 K. That this feature is indeed magnetic in origin was confirmed by the

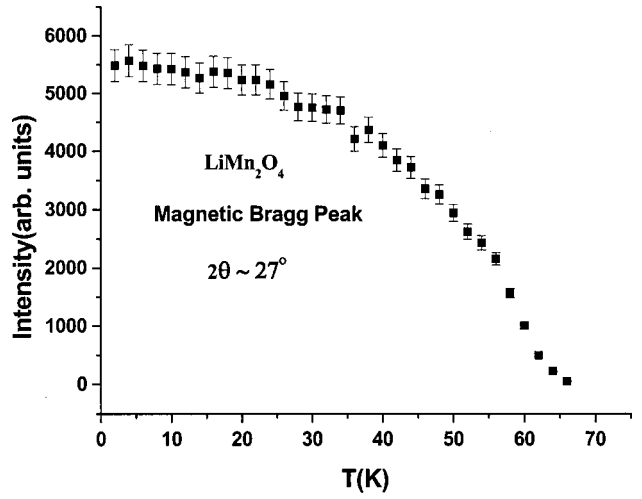

FIG. 3. The temperature dependence of the intensity of the magnetic peak at $2\theta \sim 27°$ for $LiMn_2O_4$.

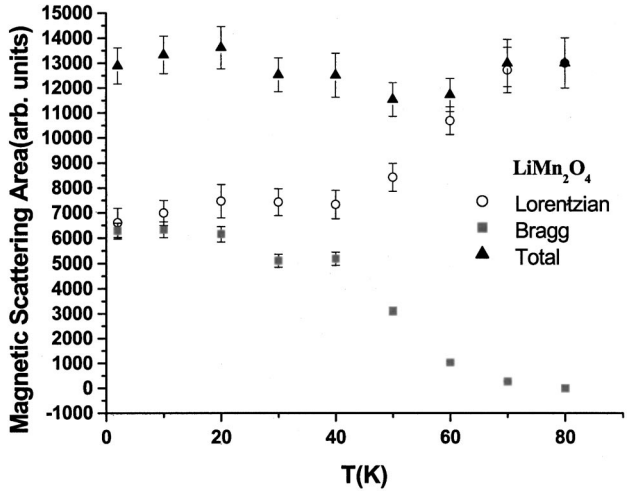

FIG. 4. Temperature dependence of the Bragg (LRO) and Lorentzian (SRO) components of the magnetic cross section and their sum for $LiMn_2O_4$, D1B (unpolarized neutron) data.

neutron polarization analysis measurements. An attempt was made to separate the total magnetic scattering between the Bragg and diffuse components. The Bragg contribution was estimated by fitting individually the sharp features, in some cases up to 18 peaks, in each dataset to Gaussians and summing the results. The diffuse component was estimated by first subtracting the Bragg peaks from the datasets and then by fitting the resulting curve to a Lorentzian. As can be seen from Fig. 4, all of the magnetic scattering is in the Lorentzian part above T_c but this then diminishes below T_c with the corresponding development of the Bragg contribution as the temperature is decreased. Note that the total magnetic scattering, the sum of the Bragg and Lorentzian parts, is constant with temperature, i.e., it appears to be conserved within the energy window of this experiment. We note that the two components become essentially equal below 20 K, below which no further changes are observed. This suggests that on average roughly half of the spins or spin components are involved in short-range order (SRO) and the other half in long-range order (LRO) at the lowest temperatures studied.

A similar behavior has been reported in other frustrated oxides, notably the spinel, $ZnFe_2O_4$, and the related *kagomé* jarosites, $KM_3(SO_4)_2(OD)_6$, $M = Fe^{3+}$ and Cr^{3+}, in which coexisting Bragg and diffuse magnetic scattering have been observed.[24–28] The pyrochlore lattice which is found in the spinels can be constructed by stacking of *kagomé* layers in an *ABCABC* manner.[29] For $ZnFe_2O_4$ the diffuse component comprises ~15% of the total magnetic scattering at 4.2 K, T_N for this material being 10.5 K. For $LiMn_2O_4$ at the same T/T_c of 0.4, the diffuse fraction is much higher, ~55%. There are of course a number of significant differences between $ZnFe_2O_4$ and the manganate spinel. The former remains cubic down to the lowest temperatures, thus, there is only one Fe site, and the Fe atoms have an integral oxidation state of +3.0. Consequentially, it does not possess the spin-related disorder present in $LiMn_2O_4$. The jarosites, on the other hand, generally show significant site disorder on the magnetic sublattice, which of course favors the establish-

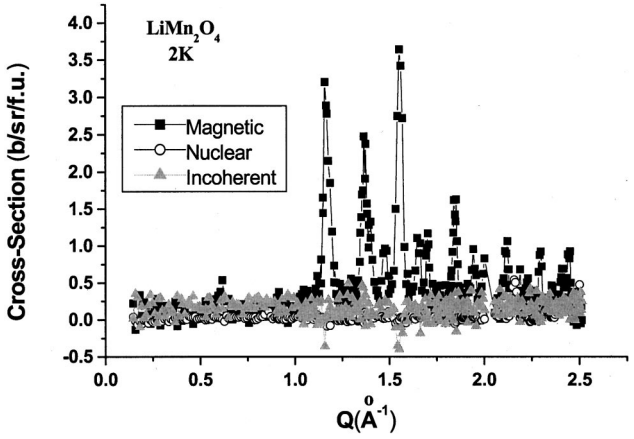

FIG. 5. The nuclear, spin-incoherent and magnetic contributions to the total scattering for $LiMn_2O_4$ at 1.5 K from *xyz* polarization analysis, D7 data.

ment of short-range order. For example, $KFe_3(SO_4)_2(OD)_6$ orders at 65 K but at 1.5 K the diffuse fraction is still finite.[26] There is a ~10% vacancy concentration on the Fe site in this material. The Cr jarosite orders at 1.8 K and even at 400 mK the diffuse fraction is large. For this compound the vacancy concentration at the magnetic site is even greater, ~24%.[28]

B. Neutron polarization analysis

XYZ polarization analysis allows the nuclear, spin-incoherent, and magnetic components to the total scattering to be determined simultaneously. Figure 5 shows the three contributions for the investigated *Q* range at 1.5 K. It is clear that the features seen in the unpolarized neutron data are indeed magnetic in origin. Although the D7 data are flux limited due to the polarization analysis and the statistics are poorer than the D1B data, it was possible to estimate the contributions of the diffuse and Bragg components in the manner described in the previous section. The result is essentially the same, the fraction SRO/(SRO+LRO) $=0.46(6)$ at 1.5 K.

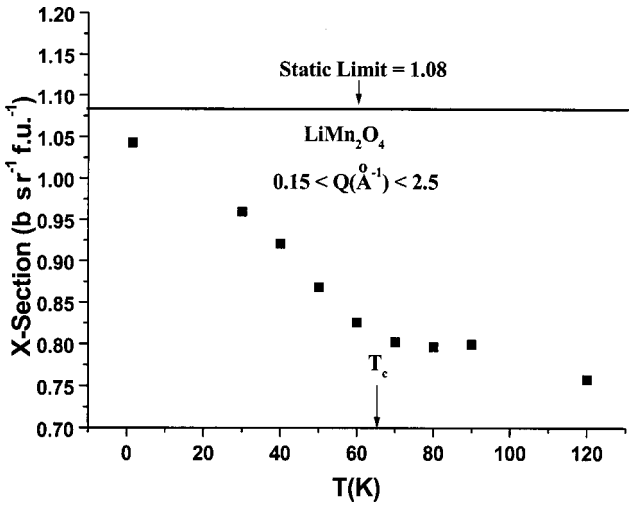

FIG. 6. Temperature dependence of the total magnetic cross section, $d\sigma_{\text{magn}}\backslash d\Omega$ for $LiMn_2O_4$. $T_c=65$ K is marked as is the static spin limit.

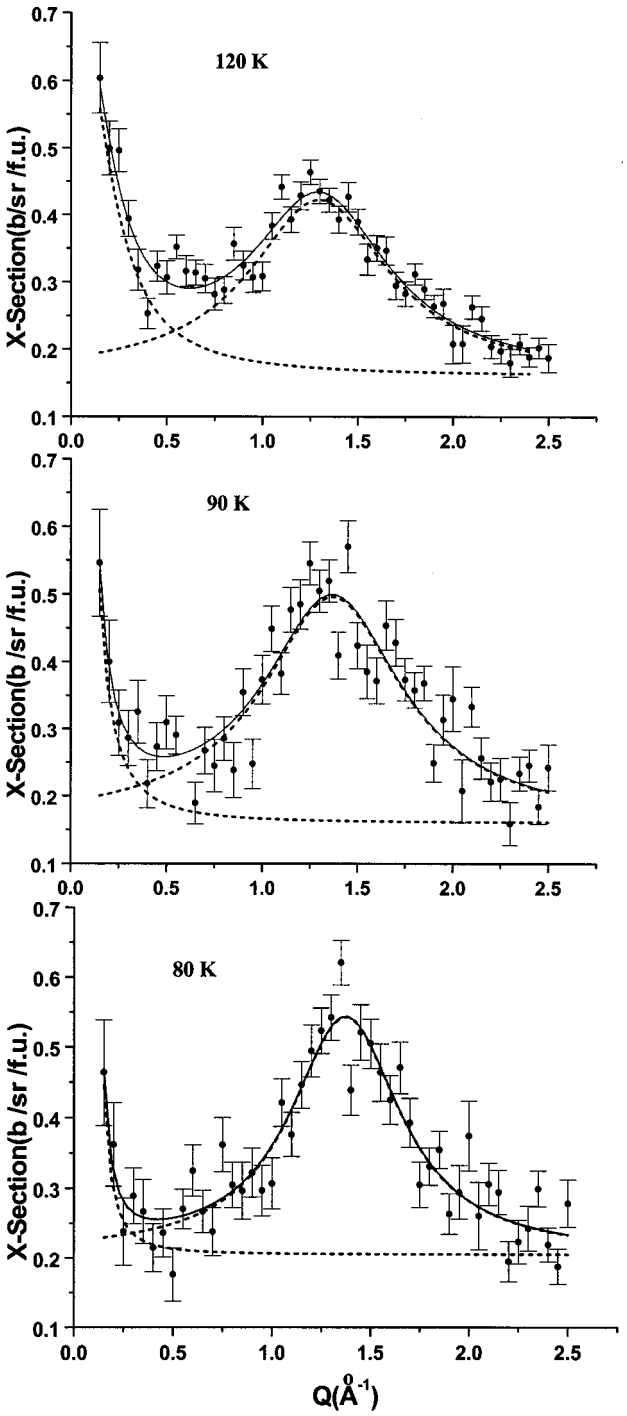

FIG. 7. Magnetic diffuse scattering for $LiMn_2O_4$ above T_c showing the development of the SANS tail with increasing temperature. The dashed lines are fits to two separate Lorentzians.

The quantitative nature of the D7 data allows the determination of the total magnetic differential cross section within the experimental energy window, $d\sigma_{\text{magn}}\backslash d\Omega$, at each temperature by integration over the wave-vector transfer, **Q**. These results are given in Fig. 6 from 120 K (~$2T_c$) to 1.5

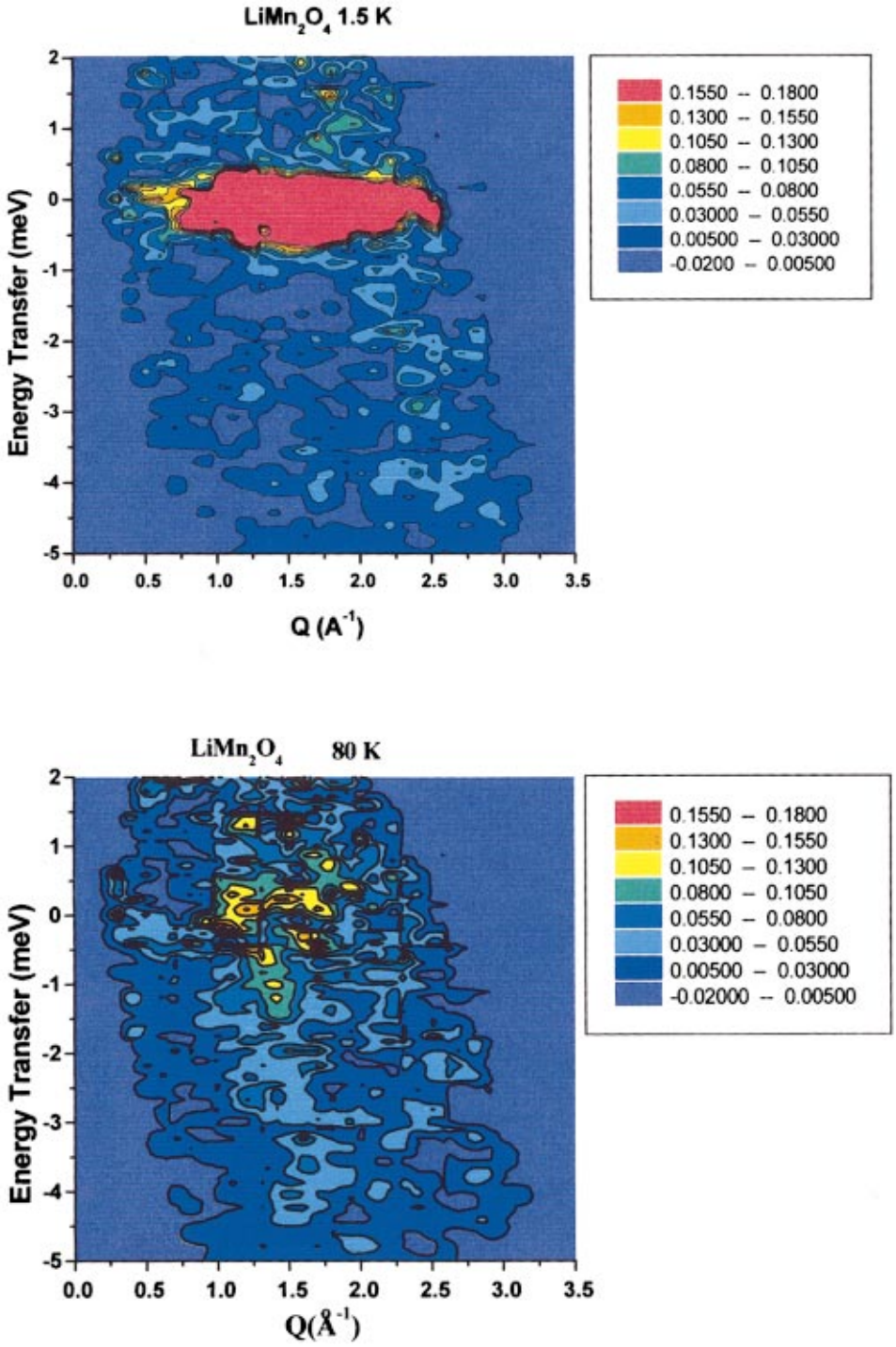

FIG. 8. (Color) Inelastic neutron scattering data with neutron polarization analysis for $LiMn_2O_4$ at 1.5 and 80 K.

K. At 1.5 K $d\sigma_{\text{magn}}\backslash d\Omega$ reaches a value of 1.05 b sr^{-1} f.u.$^{-1}$. There are two limiting cases for describing the magnetic cross section, which can be termed the dynamic or paramagnetic limit and the static or frozen-spin limit. For the dynamic case,[30]

$$d\sigma_{\text{magn}}\backslash d\Omega = 2/3 \times 0.29 \times f(Q)^2 \times S(S+1),$$

where the factor 0.29 is comprised of some fundamental constants and assumes that $g=2$, $f(Q)$ is the form factor for the ion in question and S is the spin quantum number. For $LiMn_2O_4$ this value is 1.68 b sr^{-1} f.u.$^{-1}$. In the static limit, $S(S+1)$ is replaced by S^2 and the calculated value for $LiMn_2O_4$ is 1.08 b sr^{-1} f.u.$^{-1}$. This latter value for a model of frozen spins is in excellent agreement with the measured cross section. It, therefore, provides strong evidence for the coexistence of both states with static long-range and short-range order in $LiMn_2O_4$ at 1.5 K. Figure 6 also shows a $\sim$30% increase in $d\sigma_{\text{magn}}\backslash d\Omega$ over the temperature range of the experiment and that most of this increase occurs below T_c. This indicates that significant magnetic scattering occurs outside of the experimental energy window above T_c, which

is shifted back into the measurable range below T_c, i.e., as the magnetic correlations become more static. At first glance these results appear to be in conflict with those of Fig. 4, but the latter data were obtained with much more energetic neutrons, $\lambda = 2.52$ Å (12.9 meV) and, hence, a much wider energy window, compared with $\lambda = 4.8$ Å (3.55 meV) used in the neutron polarization analysis experiments.

In Fig. 7 the magnetic scattering above T_c is displayed. Even at 120 K, $T \approx 2T_c$, the diffuse peak is still prominent. As T_c increases from 80 to 120 K, the peak position shifts from 1.36 to 1.29 Å^{-1} and the width increases from 0.68(1) Å^{-1} to 0.89(13) Å^{-1}. The position of the diffuse peak at 80 K corresponds to a d spacing of 4.62 Å, which is not obviously related to any high-symmetry direction in the low-temperature supercell. From the peak width a spin-spin correlation length, $\xi = 3(1)$ Å, is derived. This is of the order of nn Mn-Mn distances which indicates the very short range nature of the correlations in contrast to for example $ZnFe_2O_4$ for which $\xi = 13-16$ Å has been reported and $KFe_3(SO_4)_2(OD)_6$, $\xi \sim 19$ Å.[25,27]

We note the presence of another feature in the data of Fig. 7, a low-Q tail that increases in magnitude with increasing temperature. This SANS (small-angle neutron scattering) like component is estimated to comprise ~5% of the total magnetic scattering at 80 K, ~11% at 90 K and ~26% at 120 K. As, from Fig. 6, the integrated magnetic scattering intensity does not change much over this temperature range, it is clear that a significant fraction of the magnetic scattering is transferred to the low-Q component with increasing temperature. The origin of this low-Q contribution is unclear. Simple paramagnetic scattering can be ruled out due to the very strong Q dependence displayed. A natural interpretation would be to assign this to a short-range ferromagnetic component but this is incompatible with the absence of depolarizing effects in the polarized neutron scattering data unless the correlation length is very small, <20 Å. There is, however, a more likely explanation.

A similar low-Q feature has been seen in a related material, SCGO ($SrCr_8Ga_4O_{19}$), from data on the D7 instrument.[31] In this case the SANS-like feature was attributed as a manifestation of the effects of inelastic scattering on the Q-spectrum in the elastic mode of D7. On direct-geometry TOF inelastic neutron spectrometers such as D7, the Q,ω trajectory of a detector at a constant angle is such that the energy transfer and Q are related as

$$\frac{\hbar^2|\mathbf{Q}|^2}{2m} = 2E_i - \Delta E - 2\cos(2\theta)\sqrt{E_i(E_i-\Delta E)},$$

where E_i is the incident neutron energy, ΔE is the energy transfer, and θ is the angle of the detector in question. The nominal value of **Q** in a neutron diffraction measurement is given as the value at the elastic line, calculated by setting $\Delta E = 0$. Therefore, as the spin fluctuations at some constant **Q** become more dynamic and the spectral weight shifts to higher energy transfers, this intensity will appear at a lower detector angle causing an apparent small-angle scattering feature. This interpretation is consistent with the picture presented previously in the context of the temperature dependence of the elastic cross section, i.e., in which the level of spin dynamics at energy transfers outside of the experimental window increases with increasing temperature.

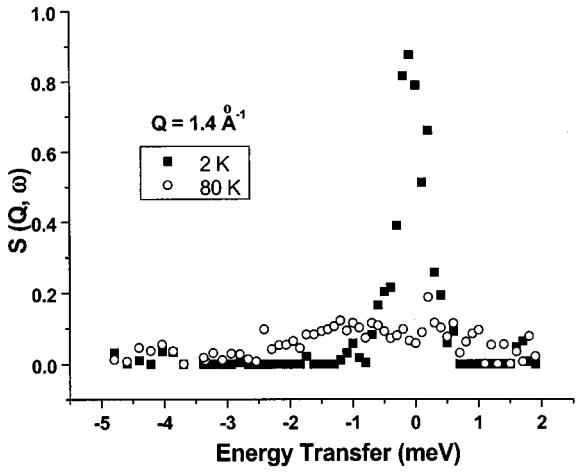

FIG. 9. Comparison of 1.5 and 80 K inelastic data for $LiMn_2O_4$ at constant $Q = 1.4$ Å^{-1}.

C. Inelastic scattering with neutron polarization analysis

The results of the inelastic, TOF measurements are displayed in Fig. 8 for both 1.5 and 80 K. It is apparent that the scattering is essentially elastic at 1.5 K and this is verified by comparison with the instrumental resolution obtained from a vanadium measurement. In contrast, the scattering at 80 K is spread over a wide energy-transfer range and is significantly weaker as illustrated in Fig. 9 where the energy spectrum for $Q = 1.4$ Å^{-1} is shown. Indeed, the data at 80 K appear to be essentially quasielastic. This result is qualitatively similar to that presented in Ref. 18. However, it should be noted that the sample studied in that work did not show Bragg peaks even at 8 K. These results can also be compared with those for $ZnCr_2O_4$.[32] Here the data above T_c are similar to those for $LiMn_2O_4$ but below T_c, 12.5 K, a localized spin resonance was seen at 4.5 meV for 1.7 K. No such resonance is seen for $LiMn_2O_4$, at least over the same range of energy transfer.

The data of Fig. 8 were integrated over ω for both temperatures. At 1.5 K where the scattering is essentially elastic, the differential cross section obtained was 1.09 b sr^{-1} f.u.$^{-1}$, while the integrated area was much less at 80 K, 0.67 b sr^{-1} f.u.$^{-1}$. Thus, ~38% of the total scattering moves outside of the energy window upon increasing the temperature from 1.5 to 80 K. This is a larger decrease than that seen in the elastic scattering experiment where a ~23% deficit was observed. This apparent discrepancy is due to the narrower energy window for the TOF configurations of the instrument.

An attempt was also made to separate the scattering at both temperatures into an elastic and an inelastic contribution. To this end, an ''elastic box'' was defined with the limits $0.4 < Q < 2.8$ Å^{-1} and $-0.62 < \omega < 0.73$ meV within which the intensity was set to zero and the integration was carried out over the remainder of the accessible Q, ω space. The 1.5 K data, which appear to be substantially elastic, were used as

a guide in determining the box dimensions and this introduces a degree of arbitrariness. Application of this procedure gives for 1.5 K, 0.25 $\mathrm{b\,sr^{-1}\,f.u.^{-1}}$ and for 80 K, 0.51 $\mathrm{b\,sr^{-1}\,f.u.^{-1}}$. Given the limitations of the procedure described, one can then estimate the fraction of fluctuating moment at 80 K to be at least 75% and at 1.5 K to be at most 23%.

IV. CONCLUSIONS

The picture that emerges of $LiMn_2O_4$ is that of a cooperative paramagnet, given the evidence for short-range, dynamic, spin-spin correlations above $T_c = 65.5$ K and up to nearly $2T_c$, $T = 120$ K. Below T_c the spins gradually become static, reaching a particularly heterogeneous ground state at 1.5 K, comprised of complex LRO and SRO components involving roughly equal fractions of the available spin density. Most of the SRO component appears to be spin-glass-like but there is evidence that a small fraction of the spins, ~20%, remain dynamic even at 1.5 K. As already mentioned, the coexistence of LRO and SRO is not unusual for spinel materials but the large SRO proportion at very low reduced temperatures, ~50% for $LiMn_2O_4$ at $T/T_c = 0.02$, is unprecedented.

The occurrence of such a very complex ground state is consistent with the low-temperature chemical structure of $LiMn_2O_4$ in which only partial charge ordering occurs between Mn^{3+} and Mn^{4+}. There is, thus, apparently, sufficient charge order to support magnetic LRO but the Mn sublattice is also subject to inherent topological frustration and partial Mn^{3+}/Mn^{4+} positional disorder, conditions favorable to the stabilization of a spin-glass-like state.

ACKNOWLEDGMENTS

This work was supported by the Natural Sciences and Engineering Research Council of Canada through a Research Grant to J.E.G. C.R.W. gratefully acknowledges financial support through an NSERC PGS B and an OGSST. Ms. A. Safa-Sefat assisted with some of the data analysis. We acknowledge useful and stimulating discussions with Professor B. D. Gaulin and Dr. C. Mondelli.

[1] M. M. Thackeray, A. Decock, M. H. Rossouw, D. Liles, R. Bittihn, and D. Hoge, J. Electrochem. Soc. **139**, 363 (1992).
[2] M. M. Thackeray, J. Electrochem. Soc. **142**, 2558 (1995).
[3] P. G. Bruce, Philos. Trans. R. Soc. London, Ser. A **354**, 1577 (1996).
[4] J. B. Goodenough, Solid State Ionics **69**, 184 (1994).
[5] D. Guyomard and J.-M. Tarascon, Solid State Ionics **69**, 222 (1994).
[6] P. W. Anderson, Phys. Rev. **102**, 1008 (1956).
[7] J. Villain, Z. Phys. B **33**, 31 (1979).
[8] A. Yamada and M. Tanaka, Mater. Res. Bull. **30**, 715 (1995).
[9] Y. Shimakawa, T. Numata, and J. Tabuchi, J. Solid State Chem. **131**, 138 (1997).
[10] V. Massarotti, D. Capsoni, M. Bini, G. Chiodelli, C. B. Azzoni, M. C. Mozzati, and A. Paleari, J. Solid State Chem. **131**, 94 (1997).
[11] J. Sugiyama, T. Atsumi, A. Koiwai, T. Sasaki, T. H. Ioki, S. Noda, and N. Kamegashira, J. Phys.: Condens. Matter **9**, 1729 (1997).
[12] J. E. Greedan, N. P. Raju, A. S. Wills, C. Morin, S. M. Shaw, and J. N. Reimers, Chem. Mater. **10**, 3058 (1998).
[13] A. S. Wills, N. P. Raju, C. Morin, and J. E. Greedan, Chem. Mater. **11**, 1936 (1999).
[14] A. S. Wills, N. P. Raju, and J. E. Greedan, Chem. Mater. **11**, 1510 (1999).
[15] Y. Jang, B. Huang, F. C. Chou, D. R. Sadoway, and Y.-M. Chiang, J. Appl. Phys. **87**, 7382 (2000).
[16] C. B. Azzoni, M. C. Mozzati, A. Paleari, V. Massarotti, D. Capsoni, and M. Bini, Z. Naturforsch., A: Phys. Sci. **53A**, 693 (1998).
[17] V. Massarotti, D. Capsoni, M. Bini, P. Scardi, M. Leoni, V. Baron, and H. Berg, J. Appl. Crystallogr. **32**, 1186 (1999).
[18] Y. Oohara, J. Sugiyama, and M. Kontani, J. Phys. Soc. Jpn. **68**, 242 (1999).
[19] J. Rodriguez-Carvajal, G. Rousse, C. Masquelier, and M. Hervieu, Phys. Rev. Lett. **81**, 4660 (1998).
[20] J. Akimoto, Y. Takahashi, Y. Gotoh, and S. Mizuta, Chem. Mater. **12**, 3246 (2000).
[21] www.ill.fr/YellowBook/D7/main.html
[22] O. Scharpf and H. Capellmann, Phys. Status Solidi A **135**, 359 (1993).
[23] J. R. Stewart, K. H. Andersen, R. Cywinski, and A. P. Murani, J. Appl. Phys. **87**, 5425 (2000).
[24] Yu. G. Chukalkin and V. R. Shtirts, Sov. Phys. Solid State **30**, 1683 (1988).
[25] W. Schiessl, W. Potzel, H. Karzel, M. Steiner, G. M. Kalvius, A. Martin, M. K. Krause, I. Halevy, J. Gal, W. Schafer, G. Will, M. Hillberg, and R. Wappling, Phys. Rev. B **53**, 9143 (1996).
[26] G. S. Oakley, D. Visser, J. Frunzke, K. H. Andersen, A. S. Wills, and A. Harrison, Physica B **267-268**, 142 (1999).
[27] A. S. Wills, A. Harrison, C. Ritter, and R. I. Smith, Phys. Rev. B **61**, 6150 (2000).
[28] S.-H. Lee, C. Broholm, M. F. Collins, L. Heller, A. P. Ramirez, Ch. Kloc, E. Bucher, R. W. Erwin, and N. Lacevic, Phys. Rev. B **56**, 8091 (1997).
[29] John E. Greedan, J. Mater. Chem. **11**, 37 (2001).
[30] G. L. Squires, *Introduction to the Theory of Thermal Neutron Scattering* (Cambridge University Press, Cambridge, 1978).
[31] C. Mondelli, K. Andersen, H. Mutka, C. Payen, and B. Frick, Physica B **267-268**, 139 (1999).
[32] S.-H. Lee, C. Broholm, T. H. Kim, W. Ratcliff II, and S.-W. Cheong, Phys. Rev. Lett. **84**, 3718 (2000).